A semi-empirical Monte Carlo based model of the Detector Optical Gain of Nuclear Imaging scintillators

2012 JINST 7 P11021

(http://iopscience.iop.org/1748-0221/7/11/P11021)

PUBLISHED BY IOP PUBLISHING FOR SISSA MEDIALAB

RECEIVED: *July 11, 2012*
REVISED: *September 21, 2012*
ACCEPTED: *October 28, 2012*
PUBLISHED: *November 22, 2012*

A semi-empirical Monte Carlo based model of the Detector Optical Gain of Nuclear Imaging scintillators

D. Nikolopoulos,[a] **N. Kalyvas,**[b,1] **I. Valais,**[b] **X. Argyriou,**[a] **E. Vlamakis,**[a] **T. Sevvos**[a] **and I. Kandarakis**[b]

[a]*Department of Physics, Chemistry and Materials Science, Technological Educational Institute (TEI) of Piraeus, 122 44 Athens, Greece*
[b]*Department of Medical Instruments Technology, Technological Educational Institute (TEI) of Athens, 122 10 Athens, Greece*

E-mail: nkalyvas@teiath.gr

ABSTRACT: This paper reports a theoretical model of the optical gain of single-crystal scintillators of Nuclear Imaging. The model described the generation, propagation and escape of scintillation light as function of thickness and absorbed gamma ray energy. The latter was calculated via Monte Carlo methods at various crystal depths. The energies of 140 keV, 364 keV and 512 keV were investigated. The adopted thickness and energy values cover the range utilized in nuclear medicine imaging. For the semi-empirical approach, theoretical results were compared to experimental data for photon energies of 140 keV and 364 keV and the model's optical parameters were determined by the trial and error method. The results rendered the calculation of the optimum crystal thickness per investigated gamma ray energy. The presented results could be useful in designing nuclear medicine imaging systems.

KEYWORDS: Gamma camera, SPECT, PET PET/CT, coronary CT angiography (CTA); Models and simulations; Scintillators, scintillation and light emission processes (solid, gas and liquid scintillators); Interaction of radiation with matter

[1]Corresponding author.

doi:10.1088/1748-0221/7/11/P11021

2012 JINST 7 P11021

Contents

2012 JINST 7 P11021

1 Introduction

Scintillation is a well-known inherent process of luminescent materials whereby a characteristic light spectrum is emitted following the absorption of ionising radiation. A scintillation detector is obtained when a scintillating material is coupled to optical sensors, such as films, photocathodes, photodiodes, active matrices of amorphous silicon photodiodes and thin film transistors (a-Si/TFTs), charged coupled devices (CCDs) and complementary metal oxide semiconductors (CMOS) [1–4]. The scintillation detectors have been widely used in many technological fields from high energy and nuclear physics to industry and medical imaging [5]. Nowadays, a variety of medical imaging scintillation detectors are encountered in conventional and digital X-ray radiography, X-ray computed tomography, single-photon emission tomography (SPECT) and positron emission tomography (PET) [4–7]. The sensitivity of these systems can be increased significantly when more efficient and faster scintillating crystals are used [5, 8].

The emission of light of granular and non-granular scintillators has been investigated previously through analytical modelling [9–14]. These models take into account scintillator thickness as the main influencing parameter, while the other dimensions (e.g. area or lateral thickness) are assumed to be infinite. In addition the multiple reflections from the input and output scintillator to air interface has been modelled without taking into account the lateral dimensions of the scintillator crystal [14]. Recently, a new model was published, which accounts for the lateral thickness, however, it disregards the optical photon loss due to multiple reflections at the input and output surfaces [15]. For the application of scintillators in nuclear medicine systems, the analytical models [9–15] are insufficient in scoring gamma radiation deposited energy. This is because they

neglect energy redistribution due to scatter radiation, Compton electrons, bremsstrahlung, fluorescence photons, Auger and Koster-Cronig electrons. On the other hand, the stochastic processes of radiation transport have been studied efficiently through Monte Carlo simulation [16–28]. Several general Monte Carlo packages are available (e.g. TART, PENELOPE, MCNP, GEANT4, GATE, EGSnrcMP) [16, 17, 22, 23, 25]. Their design for complex geometries of particle showers are developed for broad uses, thus, their specialisation is constrained, unless non-trivial coding is developed with specific language or script [16, 17, 25]. Despite coding complexities, recent reports have employed general Monte Carlo packages in studying radiation and optical photon transport in medical imaging scintillators [26, 27]. In addition the effectiveness of scintillator material in terms of pixel size and for thickness values of 10 mm and 15 mm has been studied in literature [18]. Similar studies through self-developed Monte Carlo codes have been reported for X-ray scintillating granular phosphor screens [28]. The combination however of analytical optical modelling and simulation of radiation transport with general Monte Carlo codes has not been attempted for single crystal scintillators. In such an attempt, the present study employs a hybrid semi-empirical method for the estimation of the optical output of scintillator crystals in terms of Detector-Optical-Gain (DOG), i.e. the number of optical photons emitted per incident gamma ray. The method uses specially developed Monte-Carlo EGSnrc codes for scoring the gamma ray photon and energy redistribution within certain crystal scintillators. The outputs of the EGSnrc simulations are utilised as inputs into a semi-empirical analytical model which predicts DOG. Semi-empirical model adjustments are based on scintillator measurements in the energy range of Nuclear Medicine. The model is used for the estimation of the effective optical photon loss per mm. The latter parameter is employed in the estimation of an optimum scintillator thickness, between 5 mm and 25 mm, per incident gamma ray energy for the Gd_2SiO_5:Ce (GSO:Ce), Lu_2SiO_5:Ce (LSO:Ce) and $YAlO_3$:Ce (YAP:Ce) scintillators.

2 Materials and methods

2.1 Monte Carlo simulations

The EGS (Electron-Gamma-Shower) platform is a general purpose package for the Monte Carlo simulation of the coupled transport of electrons and photons in an arbitrary geometry for particles with energies above a few keV up to several hundreds of GeV [30]. The new enhanced version of EGS is called EGSnrc. EGSnrc simulates realistically the following phenomena [30]: (a) Radiation transport of electrons ($+$ or $-$) or photons in any element, compound, or mixture. (b) Bremsstrahlung production using either the Bethe-Heitler or the NIST cross sections. (c) Positron annihilation in flight and at rest (the annihilation quanta are followed to completion). (d) Multiple scattering of charged particles by coulomb scattering from nuclei using a new multiple scattering theory or accounting scattering based on the Rutherford theory or the relativistic spin effect theory. (e) Møller (e^-/e^-) and Bhabha (e^+/e^-) scattering. Exact rather than asymptotic formulae are used. (f) Continuous energy loss of charged particle tracks between discrete interactions. The total restricted charged particle stopping power consists of soft bremsstrahlung and collision loss terms. Collision loss are determined by the restricted Bethe-Bloch stopping power with Sternheimer treatment of the density effect in the general case, but with provision of using an arbitrary density effect correction. (g) Pair production (h) Compton scattering, either Klein-Nishina

2012 JINST 7 P11021

or bound Compton with or without Doppler broadening. (i) Coherent (Rayleigh) scattering (j) Photoelectric effect (k) Relaxation of excited atoms after vacancies are created (e.g. after photoelectric or Compton scattering events) to create fluorescent photons (K, L, M shells), Auger and Coster-Kronig electrons which may be tracked if requested. (l) Electron impact ionization using arbitrary theories for generating cross-sections. Five such cross-section compilations are provided in the EGSnrc distribution (Kawrakow, Casnati, Kolbenstvedt, Gryzinski, and Bote and Salvat).

The data preparation package of EGSnrcMP, PEGS4, can create data to be used by EGSnrc, using cross section tables for elements 1 through 100. In addition there are other data files which must be read in to implement many of the new options. In addition: (i) Both photons and charged particles are transported in steps of random length rather than in discrete steps. (ii) The dynamic range of charged particle kinetic energies goes from a few tens of keV up to a few hundred GeV. Conceivably the upper limit can be extended higher, but the validity of the physics remains to be checked. (iii) The dynamic range of photon energies lies between 1 keV and several hundred GeV.

All modelled scintillators were considered as single crystal blocks. These blocks were of $10 \times 10\,\mathrm{mm}^2$ entrance area and of varying z-thickness (zb-zbound). Each block was considered to be subdivided in zb equally spaced slabs of 1 mm thickness. The scintillators were considered to be exposed to radiation of 140, 364 and 511 keV initiating from a point source located at the central axis of entrance area of the first scintillator's slab. Photons generated, block distance, field size at the entrance surface and energy of the emitted X-ray quanta are definable at the beginning of every Monte Carlo run. A random number generator may calculate the direction angles of the emitted photons to scintillator block distance and field size at entrance area. In this paper normal photon incidence was simulated considering zero dimensions of this area.

2.2 Theoretical model

The theoretical model accounted for the crystal geometry and exploits the idea presented in the work of S. Zelakiewich and J. Shaw [31], where the transfer of signal in a columnar scintillator can be modeled by accounting the transmission per layer. A single-crystal scintillator of finite dimensions was considered to be irradiated at normal incidence by gamma-rays. The crystal was assumed to be divided in N layers [13, 14]. A fraction of the incident gamma-ray energy was absorbed to each layer of the crystal. Optical photons, generated at this layer, were assumed to propagate either in the forward (271° to 89°) or in the backward (91° to 269°) direction. The optical photons were propagating and loose energy in the crystal by the two following ways. Either by internal optical photon absorption in the crystal mass, or by optical photon escape when the photons were incident on the surfaces of the crystal [32]. It has been assumed that per crystal layer only a fraction, hereafter called k, was propagated to the next layer.

Let's assume a crystal scintillator of thickness T, divided into N elementary layers of thickness $\Delta t = T/N$ [13, 15]. In each elementary layer, at position n, a fraction of the incident photon, denoted as $Q_n(E)$, deposit its energy, E. $Q_n(E)$ is calculated via the EGS4rnc Monte Carlo code. The absorbed X-ray energy is transformed into optical photon energy in the scintillator. The number of the produced optical photons in the n^{th} layer, L_n can be calculated as:

$$L_n(E) = Q_n(E) n_C \frac{E}{E_\lambda} \tag{2.1}$$

2012 JINST 7 P11021

where n_C is the intrinsic conversion efficiency and E_λ is the optical photon energy [5, 8]. It is assumed that half of the produced optical photons are propagating forward and half backwards. The forward propagated optical photons are subjected to absorption in the crystal material. In addition the lateral propagated photons at angles near 271° and 89° may escape the crystal [32]. Thus, to the next layer, $n+1$, only a fraction, k, of the produced optical photons arrives. That is:

$$L^n_{n+1}(E) = L_n(E)k \tag{2.2}$$

2.3 Forward direction

If the $N-n$ layers to the crystal output is considered then:

$$L^n_{N-n}(E)_f = L_n(E)k^{N-n} \tag{2.3}$$

If R is an average reflectance for all incident angles to the output layers, then a fraction, $(1-R)$ $L^n_{N-n}(E) = (1-R)L_n(E)k^{N-n}$, escapes to the output and the rest $RL_n(E)k^{N-n}$, suffers reflection and propagates backwards. When the reflected backward fraction arrives to the input surface of the crystal it has subjected to optical photon loss equals to k^N. Therefore the total number of the optical photons arriving at the input equals to $L_n(E)k^{N-n}Rk^N$. From the input surface, a fraction of the photons is again reflected back to the output, equals to $L_n(E)k^{N-n}Rk^NR$, and after suffering a reduction by k^N, number of photons equals to $L_n(E)k^{N-n}Rk^NRk^N$, reflects or transmits to the output. Thus the number of the optical photons transmitted to the output from the initial reflection and the first travel can be calculated as $(1-R)L_n(E)k^{N-n} + L_n(E)k^{N-n}Rk^NRk^N(1-R)$. By assuming multiple reflection travels to the output-input boundaries the total number of the optical photons $L_{nf}(E)_f$ escaping to the output equals to:

$$L_{nf}(E) = (1-R)L_n(E)k^{N-n} + (1-R)L_n(E)k^{N-n}k^Nk^NRR + (1-R)L_n(E)k^{N-n}k^Nk^Nk^Nk^NRRRR + \cdots \tag{2.4}$$

By rearranging the terms, equation (2.4) can be written as:

$$\begin{aligned} L_{nf}(E) &= (1-R)L_n(E)k^{N-n}\left[1 + k^{2N}R^2 + k^{4N}R^4 + k^{6N}R^6 + k^{8N}R^8 + \cdots\right] \\ &= (1-R)L_n(E)k^{N-n}\left[1 + \sum_{i=1}^{\infty}\left(k^{2N}R^2\right)^i\right] \end{aligned} \tag{2.5}$$

Since k is the fraction of the transmitted optical photons, it must have a value less than 1. In addition the reflection coefficient is less than one. Thus $k^2R < 1$. Keeping in mind that

$$\sum_{i=0}^{\infty}(k^{2N}R^2)^i = \frac{1}{1-k^{2N}R^2} = 1 + \sum_{i=1}^{\infty}(k^{2N}R^2)^i \tag{2.6}$$

equation (2.5) becomes:

$$L_{nf}(E) = (1-R)L_n(E)k^{N-n}\frac{1}{1-k^{2N}R^2} \tag{2.7}$$

2.4 Backward direction

If the n layers to the crystal input are considered, then the number of optical photons reaching the input surface of the crystal equals to:

$$L^n_n(E)_b = L_n(E)k^n \tag{2.8}$$

2012 JINST 7 P11021

In the backward surface, a fraction $(1-R)$ of the optical photons escape, but the rest, $RL_n(E)k^n$, propagates towards the forward surface and after passing N layers has subjected a reduction of k^N, until the output. There, a fraction $(1-R)$ escapes to the output and adds to the output signal. That is the number of the optical photons that initially propagated backwards from the n^{th} layer and arrive to the output for the first time and subsequently escape equals to $RL_n(E)k^nk^N(1-R)$. The rest, $RL_n(E)k^nk^NR$, are reflected back and suffer a loss by a factor k^N, until they reach the input surface and get equal to $RL_n(E)k^nk^NRk^N$. There a fraction R is reflected towards the forward surface, equals $RL_n(E)k^nk^NRk^NR$, suffers a subsequent loss, k^N, and reach the output, $RL_n(E)k^nk^NRk^NRk^N$and subsequently a fraction, $(1-R)$, escapes to the output, that is $RL_n(E)k^nk^NRk^NRk^N(1-R)$ and adds to the output signal. Therefore the total number of optical photons reaching the output, from the ones initially propagated backwards is:

$$\begin{aligned} L_{nb}(E) = {} & RL_n(E)k^nk^N(1-R) + RL_n(E)k^nk^NRk^NRk^N(1-R) \\ & + RL_n(E)k^nk^NRk^NRk^NRk^NRk^N(1-R) + \cdots \end{aligned} \tag{2.9}$$

By rearranging the terms equation (2.8) can be written as:

$$\begin{aligned} L_{nb}(E) &= RL_n(E)k^nk^N(1-R)\left[Rk^NRk^N + Rk^NRk^NRk^NRk^N + \cdots\right] \\ &= RL_n(E)k^nk^N(1-R)\left[\sum_{i=1}^{N}(R^2k^{2N})^i\right] \end{aligned} \tag{2.10}$$

Similar to the previous paragraph:

$$\begin{aligned} L_{nb}(E) &= RL_n(E)k^nk^N(1-R)\left[\sum_{i=1}^{N}(R^2k^{2N})^i\right] \\ &= RL_n(E)k^nk^N(1-R)\left[\frac{1}{1-R^2k^{2N}} - 1\right] \\ &= RL_n(E)k^nk^N(1-R)\frac{R^2k^{2N}}{1-R^2k^{2N}} \end{aligned} \tag{2.11}$$

Thus the total number of optical quanta from the ones generated at the n^{th} layer and escaping to the output equals to:

$$L_m(E) = L_{nf}(E) + L_{nb}(E) = (1-R)L_n(E)k^{N-n}\frac{1}{1-k^{2N}R^2} + (1-R)L_n(E)Rk^nk^N\frac{k^{2N}R^2}{1-k^{2N}R^2} \tag{2.12}$$

If all the layers as well as equation (2.1) are considered then the total number of optical photons produced per absorbed gamma ray (i.e. DOG) equals to:

$$\text{DOG}(E) = \sum_{n=1}^{N} Q_n(E)n_C\frac{E}{E_\lambda}(1-R)\left[\frac{k^{N-n}}{1-k^{2N}R^2} + Rk^{n+N}\frac{k^{2N}R^2}{1-k^{2N}R^2}\right] \tag{2.13}$$

where the values of $Q_n(E)$ is calculated by EGSnrcMP.

The value of the reflectance, R, when a light ray propagates from a medium with index of refraction n_1, to a medium of index of refraction n_2 (equals to 1 for air), depends upon the polarization of the incident ray. Therefore for the s-polarized component and the p-polarized component [33]:

$$Rs(\theta i) = \left[\frac{n_1\cos\theta i - n_2\sqrt{1-\left(\frac{n_1}{n_2}\sin\theta i\right)^2}}{n_1\cos\theta i + n_2\sqrt{1-\left(\frac{n_1}{n_2}\sin\theta i\right)^2}}\right]^2 \tag{2.14}$$

2012 JINST 7 P11021

Table 1. Physical properties of the scintillators studied.

Crystal	Dimensions (mm×mm×mm)	E_λ (eV)	n_C	Effective Z	Density (g cm^{-3})	Index of refraction
LSO:Ce	10×10×10	2.95	0.082	64.76	7.40	1.82
GSO:Ce	10×10×10	2.82	0.022	57.55	6.71	1.80
YAP:Ce	10×10×20	3.54	0.074	32.27	5.37	1.92

and

$$Rp(\theta i) = \left[\frac{n_1\sqrt{1-\left(\frac{n_1}{n_2}\sin\theta i\right)^2} - n_2\cos\theta i}{n_1\sqrt{1-\left(\frac{n_1}{n_2}\sin\theta i\right)^2} + n_2\cos\theta i}\right]^2 \tag{2.15}$$

The total reflectance can be calculated as $R(\theta i) = Rs(\theta i) + Rp(\theta i)/2$ and the mean reflectance used in the estimation of equation (2.13) was found as $R = \frac{\sum_{\theta=0}^{\theta_{\text{crit}}} R(\theta)}{\text{noa}}$, where noa is the number of angles used in the summation and θ_{crit} is the critical angle above which total reflection occur. In the calculation of R it was assumed that the input and exit surfaces of the crystal were perfect planes and any existed surface anomalies [26] were not considered.

2.5 Experiments

The experimental DOG values were obtained from the literature [8]. The experimental method comprised irradiation by radioisotope energies of Tc99m (140 keV) and I131 (364 keV). Light energy flux was measured by a calibrated photomultiplier (EMI 9798B) equipped with an extended sensitivity S-20 photocathode. For each measurement the exposure was calculated by considering the specific gamma correction, Γ, factor for each isotope. That is $\Gamma_{\text{Tc99m}} = 0.61\,\text{mRh}^{-1}\text{mCi}^{-1}$ and $\Gamma_{\text{I131}} = 2.16\,\text{mRh}^{-1}\text{mCi}^{-1}$. To avoid unnecessary radiation exposure, the radioisotope was enclosed in a glass vial and was handled via appropriate cylindrical lead shield. The bottom of the cylinder, which was irradiating the scintillator crystal was unshielded. In table 1 some physical properties used in equations (2.1)–(2.15) are demonstrated.

Equation (2.13) was fitted by the trial and error method, to the DOG experimental results, presented in table 1, using the value of k as a free variable. During the fitting procedure the R calculated were 0.12 for LSO:Ce, 0.11 for GSO:Ce and 0.12 for YAP:Ce. The k value obtained was used to predict the DOG values of LSO:Ce, GSO:Ce and YAP:Ce of various thickness values in order to determine an optimum crystal thickness.

3 Results and discussion

The $Q_n(E)$ values of the crystals, used in equation (2.13), simulated by EGSnrcMP are presented in figure 1. The errors of the simulations were estimated by 15 independent iterations under identical conditions. All estimated errors are below 0.5%. It can be observed from figure 1, that the energy absorbed fraction is larger in the early crystal layers for the gamma ray energies of 140 keV while in the energy of 364 keV the percentage per layer is relative constant. The absolute $Q_n(E)$ values

2012 JINST 7 P11021

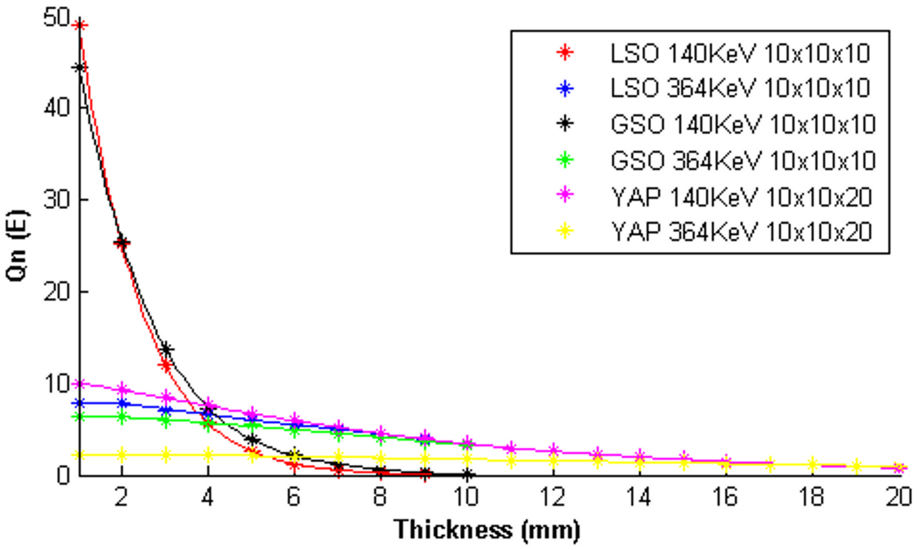

Figure 1. The calculated percent energy absorption fractions, $Q_n(E)\%$, for gamma ray energies of 140 keV and 364 keV for LSO:Ce, GSO:Ce and YAP:Ce. The curves represent exponential fits at the 99% confidence interval. The errors are below 0.5%. The legend presents the dimensions of the modeled scintillator block.

Table 2. Experimental and semi-empirical method predicted DOG values. In the last two columns the sensitivity of the method in k values is demonstrated.

Crystal	Energy (keV)	DOG experimental	k	DOG theoretical	DOG $k-1\%$	DOG $k+1\%$
LSO:Ce	140	323 ± 16	0.80	248	227	271
	364	644 ± 45		790	753	828
GSO:Ce	140	150 ± 8	0.86	146	133	160
	364	275 ± 19		291	275	308
YAP:Ce	140	57 ± 3	0.74	50	48	54
	364	95 ± 7		111	107	117

are dependent upon the density and the effective Z of the material, as shown in table 1 [22, 34], which affects the type of gamma photon interaction and energy deposition. It is of importance to denote that for low effective Z and low density materials (i.e. YAP) the energy deposited can be up to five times smaller than higher Z materials. It is evident from figure 1 that the absorption of gamma energy in each slab follows approximately the exponential law. This is of importance since it indicates non-significant degradation of $Q_n(E)$ due to self-absorption or side transmittance. This accordingly implies that the employed thickness range is adequate for Nuclear Imaging investigation. Higher scintillator thickness values may necessitate consideration of multiple readout layers, phoswichs etc. The latter could result significant spatial resolution degradation in reconstructed images produced by using longer crystals.

In table 2 the corresponding DOG values [8] for the crystals under investigation is shown. It can be observed that the predicted results are in good (i.e. GSO:Ce) or at least fair (i.e. LSO:Ce

2012 JINST 7 P11021

Table 3. Experimental and semi-empirical method predicted DOG values for 140 keV irradiation conditions. The experimental values are from ref. [35]. The optical photon energy has been calculated from the peak emission wavelength.

Crystal	AE (μW·s/mR·m^2)	Eλ (eV)	DOG experimental at 140 keV
LSO:Ce	24.18	2.95	323
GSO:Ce	10.7	2.88	147
YAP:Ce	9.13	3.35	108

and YAP:Ce) agreement with the corresponding experimental results. An explanation for the differences could possibly rely on experimental errors (i.e. misalignment of the vial its shield and the scintillator). In order to examine if there were simulation inconsistencies between the Monte Carlo narrow beam geometry and the real experimental conditions, numerous Monte Carlo simulations of varying irradiation geometry were performed. The error was found below 1% for the 10^6 iterations employed in the simulation. On the other hand, significant errors, above 5%, may be induced if less than 10^6 iterations are employed. More than 10^6 iterations impose minimal alterations, viz., on the order of 0.1%, possibly, due to the variance reduction techniques applied. In addition in table 3 the corresponding DOG values for LSO:Ce, GSO:Ce and YAP:Ce for 140 keV, obtained from other published literature [35] are also presented. The calculation method is described in the appendix. The incident radiation in [35] is directly measured in air kerma units (mGy), instead of calculating exposure (mR) in terms of the radiation gamma factor of the radioisotope. Therefore the DOG values obtained using the method presented in [35] should take into account the relation between air kerma and exposure, in order the DOG values to have units of optical photons emitted per incident gamma ray photon (see appendix). The difference in experimental DOG values for YAP:Ce may be attributed in differences in the experimental setup and procedures. The corresponding k value for the YAP:Ce obtained from reference [35] equals to 0.821.

A point worth mentioning is that the corresponding values of k correspond to crystals of the specific polish surface technique, since crystals with all the lateral planes polish tends to diminish the effect of the optical photon diffraction from the lateral surfaces and allow a larger percentage of the optical photons (i.e. k value) to be transmitted to the next layer of the scintillator. The last two columns of table 2 demonstrate the sensitivity of the model to k. It may be observed that a change of 1% in the value of k yields changes ranging from 5% to 10% of the predicted DOG values. Finally it may be observed from table 1 and table 2 that the value of k for each crystal is more a function of the index of refraction, than the peak energy of the optical photon spectrum. This accordingly implies that the light losses from layer to layer can be attributed more to the lateral light escape by the crystal, than the interactions of the optical photons in it.

In figures 2(a), 2(b) and 2(c) the predicted DOG values for crystal thickness values of 5, 7, 10, 12, 15, 20 and 25 mm are demonstrated. The errors of the estimations are given only for the 140 keV curves to avoid misidentification of data points and correspond to 18% for LSO:Ce, 5% for GSO:Ce and 8% for YAP:Ce. It can be observed that for Tc99m applications (140 keV) the optimum crystal thickness is 5 mm for every scintillator type. For PET applications (512 keV) an

2012 JINST 7 P11021

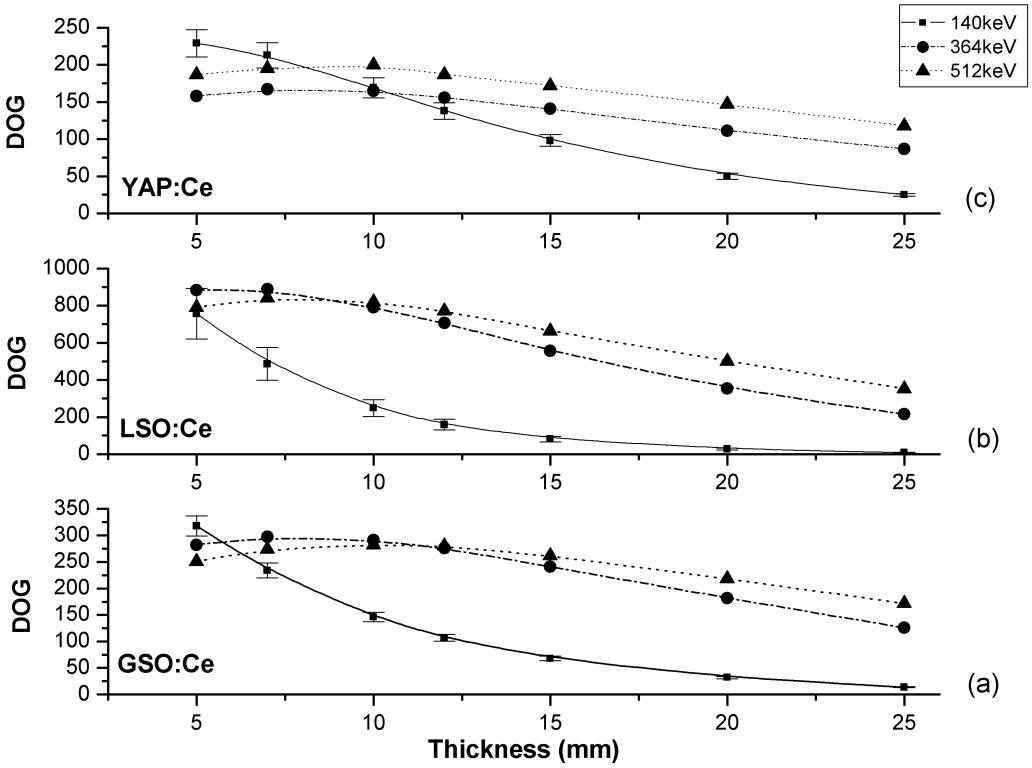

Figure 2. The predicted DOG values for different scintillator total thickness (T) and gamma ray energies of 140 keV, 364 keV and 512 keV for (a) GSO:Ce, (b) LSO:Ce and (c) YAP:Ce.

optimum crystal thickness of 10 mm for GSO:Ce, 7 mm for LSO:Ce and 10 mm for YAP:Ce is observed. This optimum thickness is derived by the fact that a high crystal thickness, although enhances energy absorption, allows more optical photon loss during propagation to the output. It can also be observed that for the 364 keV and 512 keV energies, the LSO presents higher DOG values from the other crystals. For the 140 keV energy however the DOG values of YAP:Ce were found higher from the other crystals, for thickness values above 15 mm, as presented in figure 3. This may be explained by the fact that due to its lower effective Z value and as observed in figure 1 the energy deposited in YAP is higher in layers far from the input surfaces than that of the other crystals. It is worth mentioning that figure 2 may be of value for finding the thickness with the highest DOG value (optimum thickness) per gamma ray energy. By examining figures 2 it may be deduced that the optimum thickness for LSO:Ce is 7 mm, for GSO:Ce and YAP:Ce are 7 mm for 364 keV and 10 mm for 512 keV. The thickness values calculated are dependent upon the corresponding $Q_n(E)$ values, describing gamma ray energy absorption, as well as the calculated k value describing the fraction of the optical photons that are not subjected to absorption or escape from the lateral surfaces of the scintillator.

4 Conclusion

A semi-empirical theoretical model, describing light transport in single crystals was developed. The model was used in conjunction with a Monte Carlo generated gamma ray absorption data

2012 JINST 7 P11021

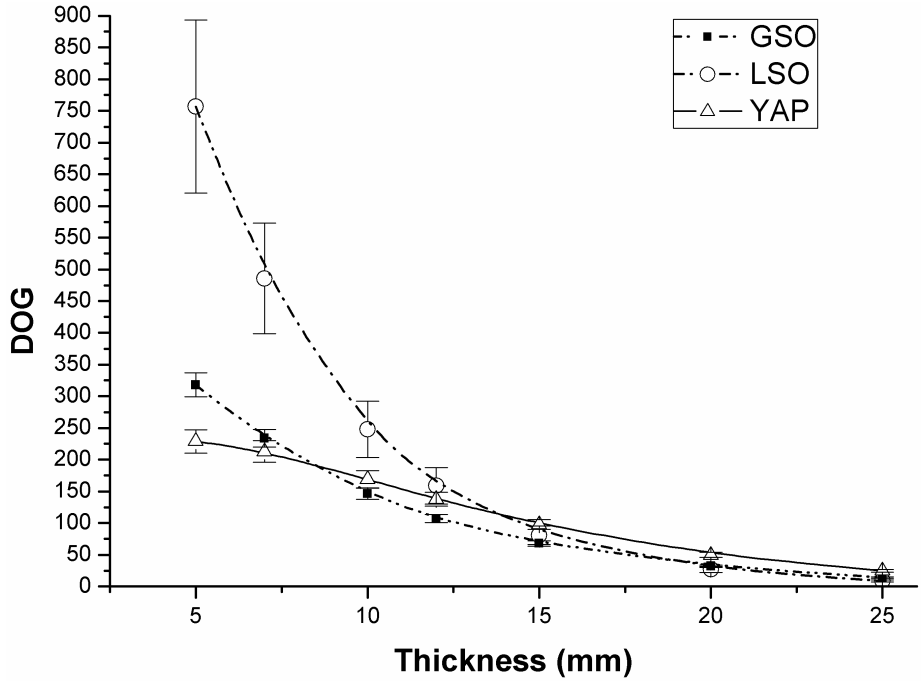

Figure 3. The predicted DOG values of GSO:Ce, LSO:Ce and YAP:Ce for gamma ray energy of 140 keV.

to describe the Detector Optical Gain (DOG) of single crystal scintillator materials excited by gamma rays. The model was checked against experimental results and the fraction of the optical photons propagating through crystal layers (named k) was determined. The model was used to find an optimum crystal thickness per gamma ray energy application. It was found that the optimum thickness is a function of the scintillator material and the gamma ray energy.

A DOG calculation from absolute efficiency experimental data

Absolute efficiency, AE, is defined as the ratio of the light energy flux emitted by the scintillator over the incident radiation exposure (in units μWs/mRm^2), that is [8, 35]:

$$\mathrm{AE} = \frac{\dot{\Phi}_\lambda}{\dot{X}} \tag{A.1}$$

The emitted light energy flux equals to

$$\Phi_\lambda = N_\lambda E_\lambda \tag{A.2}$$

where N_λ is the number of the optical photons emitted per unit area and E_λ is the optical photon energy.

If the definition of X-ray exposure is considered then [36]:

$$X = N_\gamma E_\gamma \left(\frac{\mu_{\mathrm{en}}}{\rho}\right)_{\mathrm{air}} \left(\frac{e}{W}\right)_{\mathrm{air}} \tag{A.3}$$

where N_γ is the number of gamma photons per unit area, E_γ is their corresponding energy, $\left(\frac{\mu_{\mathrm{en}}}{\rho}\right)_{\mathrm{air}}$ is the mass energy absorption coefficient of air for energy E_γ and equals to 2.46×10^{-2} cm^2/g [34]

and $\left(\frac{W}{e}\right)_{\text{air}}$ is the energy required per unit charge of ionization occurred and equals 33.97 J/C and 1R equals 2.58×10^{-4} C/Kg. If one considers the definition of DOG, then:

$$\text{DOG} = \frac{N_\lambda}{N_\gamma} = \text{AE}\frac{N_\gamma E_\gamma \left(\frac{\mu_{\text{en}}}{\rho}\right)_{\text{air}} \left(\frac{e}{W}\right)_{\text{air}}}{N_\gamma E_\lambda} = \text{AE}\frac{E_\gamma}{E_\lambda}\left(\frac{\mu_{\text{en}}}{\rho}\right)_{\text{air}}\left(\frac{e}{W}\right)_{\text{air}} \tag{A.4}$$

That is DOG in units of optical photons per incident X-ray photon can be determined by measurements of AE, provided that AE is calculated with regards to radiation exposure.

If AE is calculated with regards to incident air kerma (mGy) as in reference [35], the corresponding DOG value may be translated in optical photons per incident gamma-ray photon, if the air kerma, K_{air} is converted to exposure, where

$$K_{\text{air}}(\text{cGy}) = 0.876\left(\frac{cCy}{R}\right) \cdot X(R) \tag{A.5}$$

The AE values for 140 keV for GSO:CE, LSO:Ce and YAP:Ce are 1221.29 μW·s/mGy·m^2, 2759.79 μW·s/mGy·m^2 and 1042.5 μW·s/mGy·m^2 respectively [35]. The corresponding values, if the mGy are translated in mR by using equation (A.5), are demonstrated in table 3. If equation (A.4) is used for $E_\gamma = 140$ keV and E_λ equals to 2.95 eV for LSO:Ce, 2.88 eV for GSO:Ce and 3.35 eV for YAP:Ce, then the corresponding DOG values in units of optical photons emitted per incident gamma photon are also demonstrated in table 3.

References

[1] O. Mineev, Y. Kudenko, Y. Musienko, I. Polyansky and N. Yershov, *Scintillator detectors with long WLS fibers and mulit-pixel photodiodes*, 2011 *JINST* **6** P12004 [arXiv:1110.2651].

[2] A Vandenbroucke, A.M.K. Foudray, P.D. Olcott and C.S. Levin, *Performance characterization of a new high resolution PET scintillation detector*, *Phys. Med. Biol.* **55** (2010) 5895.

[3] B.K. Cha et al., *Design and image-quality performance of high resolution CMOS-based X-ray imaging detectors for digital mammography*, 2012 *JINST* **7** C04020.

[4] A. Nassalski et al., *Comparative study of scintillators for PET/CT detectors*, *IEEE Trans. Nucl. Sci.* **54** (2007) 3.

[5] M. Nikl, *Scintillation detectors for X-rays*, *Meas. Sci. Technol.* **17** (2006) R37.

[6] I.G. Valais et al., *Luminescence efficiency of Gd_2SiO_5: Ce scintillator under X-ray excitation*, *IEEE Trans. Nucl. Sci.* **52** (2005) 1830.

[7] I.G. Valais et al., *Luminescence properties of $(Lu,Y)_2SiO_5$:Ce and Gd_2SiO_5:Ce single crystal scintillators under X-ray excitation for use in medical imaging systems*, *IEEE Trans. Nucl. Sci.* **54** (2007) 11.

[8] I.G. Valais, *Systematic study of the light emission efficiency and the corresponding intrinsic physical characteristics of single crystal scintillators, doped with the trivalent cerium (Ce^{3+}) activator, in wide energy range (from 20 kV–18 MV) for medical applications*, Ph.D. Thesis, University of Patras (2008), http://nemertes.lis.upatras.gr/jspui/bitstream/10889/997/1/Thesis_Valais_sec.pdf.

[9] G.E. Giakoumakis and C.D. Nomicos, *Light angular distribution of non-granular fluorescent screens excited by X-rays*, *Phys. Med. Biol.* **30** (1985) 993.

2012 JINST 7 P11021

[10] G.E. Giakoumakis and D.M. Miliotis, *Light angular distribution of fluorescent screens excited by X-rays*, *Phys. Med. Biol.* **30** (1985) 21.

[11] G.E. Giakoumakis, C.D. Nomicos and P.X. Sandilos, *Absolute efficiency of Gd_2O_2S:Tb screens under fluoroscopic conditions*, *Phys. Med. Biol.* **34** (1989) 673.

[12] G.E. Giakoumakis, C.D. Nomicos, E.N. Yiakoumakis and E.K. Evangelou, *Absolute efficiency of rare earth oxysulphide screens in reflection mode observation*, *Phys. Med. Biol.* **35** (1990) 1017.

[13] I. Kandarakis et al., *A theoretical model evaluating the angular distribution of luminescence emission in X-ray scintillating screens*, *Appl. Radiat. Isotopes* **64** (2006) 508.

[14] C. Carrier and R. Lecomte, *Theoretical modelling of light transport in rectangular parallelepipedic scintillators*, *Nucl. Instrum. Meth.* **A 292** (1990) 685.

[15] A. Petropoulou, N. Kalyvas, I. Kandarakis, I. Valais and G.S. Panayiotakis, *A theoretical model describing the light emission efficiency of single-crystal scintillators in the diagnostic energy range*, 2009 *JINST* **4** P06016.

[16] www.opengatecollaboration.org..

[17] S. Jan et al., *GATE: a simulation toolkit for PET and SPECT*, *Phys. Med. Biol.* **49** (2004) 4543 [physics/0408109].

[18] N. Ghazanfari, S. Sarkar, G. Loudos and M.R. Ay, *Quantitative assessment of crystal material and size on the performance of rotating dual head small animal PET scanners using Monte Carlo modeling*, *Hell. J. Nucl. Med.* **15** (2012) 33.

[19] P. Gonias et al., *Validation of a GATE model for the simulation of the Siemens biograph™ 6 PET scanner*, *Nucl. Instrum. Meth.* **A 571** (2007) 263.

[20] N. Karakatsanis et al., *Comparative evaluation of two commercial PET scanners, ECAT EXACT HR+ and Biograph 2, using GATE*, *Nucl. Instrum. Meth.* **A 569** (2006) 368.

[21] Y.H. Chung etal., *Optimization of dual layer phoswich detector consisting of LSO and LuYAP for small animal PET*, *IEEE Trans. Nucl. Sci.* **52** (2005) 217.

[22] D. Nikolopoulos et al., *Investigation of radiation absorption and X-ray fluorescence properties of medical imaging scintillators by Monte Carlo methods*, *Nucl. Instrum. Meth.* **A 565** (2006) 821.

[23] D. Nikolopoulos et al., *Monte Carlo validation in the diagnostic radiology range*, *Nucl. Instrum. Meth.* **A 571** (2007) 267.

[24] B.A. Faddegon, J. Perl and M. Asai, *Monte Carlo simulation of large electron fields*, *Phys. Med. Biol.* **53** (2008) 1497.

[25] http://irs.inms.nrc.ca/software/egsnrc.

[26] D.J. (Jan) van der Laan et al., *Optical simulation of monolithic scintillator detectors using GATE/GEANT4*, *Phys. Med. Biol.* **55** (2010) 1659.

[27] F. Ciocia et al., *GEANT4 studies on the propagation and detection of scintillation light in long thin YAP crystals*, *Nucl. Instrum. Meth.* **A 600** (2009) 506.

[28] P.F. Liaparinos, I.S. Kandarakis, D.A. Cavouras, H.B. Delis and G.S. Panayiotakis, *Modeling granular phosphor screens by Monte Carlo methods*, *Med. Phys.* **33** (2006) 4502.

[29] C.W.E. van Eijk, *Inorganic scintillators in medical imaging*, *Phys. Med. Biol.* **47** (2002) R85.

[30] C.W.E. van Eijk, *Radiation detector developments in medical applications: inorganic scintillators in positron emission tomography*, *Radiat. Prot. Dosim.* **129** (2008) 13.

2012 JINST 7 P11021

[31] S. Zelakiewich and J. Shaw, *Modeling MTF and DQE for arbitrary scintillator thickness*, *IEEE Nucl. Sci. Symp. Conf. Rec.* **4** (2006) 2551.

[32] H.D. Young and F. Weston Sears, *University physics: extended version with modern physics*, 8th edition, Addison-Wesley Publishing Company Inc. (1995) [ISBN 960-02-1088-8].

[33] http://en.wikipedia.org/wiki/Fresnel_equations.

[34] R. Nowotny, *XMuDat: photon attenuation data on PC*, IAEA-NDS-195, International Atomic Energy Agency, Vienna Austria (1998).

[35] I.G. Valais et al., *Comparative investigation of Ce^{3+} doped scintillators in a wide range of photon energies covering X-ray CT, nuclear medicine and megavoltage radiation therapy portal imaging applications*, *IEEE Trans. Nucl. Sci.* **57** (2010) 3.

[36] F.M. Khan, *The physics of radiation therapy*, 2nd edition, Williams & Wilkins (1994).

2012 JINST 7 P11021